Digital holography experiment of 3D detection of underwater bubble fields

Huiping Liu (刘惠萍), Jia Yu (于 佳)*, Tian Wang (王 添), Yu Yang (杨 宇), Jincheng Wang (王金城), and Ronger Zheng (郑荣儿)

Department of Physics, Ocean University of China, Qingdao 266100, China

**Corresponding author: yujia2008@ouc.edu.cn*

Received January 28, 2013; accepted March 1, 2013; posted online August 20, 2013

Detection of underwater bubbles is one of the key issues of the research of ocean-atmosphere flux exchange. Digital holographic experiment is carried out based on Mach-Zehnder digital holographic system, to detect the distribution of bubbles. Holographic images of the dynamical bubble fields are recorded by the charge-coupled device (CCD) video system and the tomographic images at different depth are reproduced. The distribution of sizes and densities of the bubbles is obtained through following steps as denoising, edge-detection, and bubble-recognition using Hough transform. Through the experiments, the efficiency and applicability of the digital holographic detection of underwater bubble fields are tested and verified.

OCIS codes: 090.1995, 090.2880.

doi: 10.3788/COL201311.S20901.

Bubbles in the ocean is a common and important object that plays a critical role in the interchange of ocean-atmosphere fluxes such as motion, heat, and mass, etc., and also influences oceanographic remote sensing and optical detection to a large extent and thus is a key research subject in oceanography[1−3]. Exploration of bubbles in water, especially bubbles in ocean, started in 1960s[4]. The traditional methods of ebullition detection include bubble traps aided by photography[5], acoustic measurement, and optical measurement methods. The acoustic method, which is widely used[2,6], treats a huge amount of bubbles as one 'cloud' and therefore does not find the information of any individual bubble. Moreover it cannot distinguish bubbles from other particles. Common two-dimensional (2D) optical imaging is also used in detection of water bubbles[7], however it has significant errors caused by perspective as the sizes of the recorded bubbles vary with depths of field needless to say that the bubbles overlap each other. O' Hern *et al.*[8] used laser holography to detect the three-dimensional (3D) information of bubbles in given volume of ocean water in one exposure with high efficiency and shown that the radii bubbles vary from 10 to 15 μm. However traditional holography is not really applicable for the situ investigation as it requires pulsed laser with high power, highly stable instruments, and chemical post-processing. With the development of computer science and digital images technology, digital holography is used in particle field studies[9−13]. This technique inherits the advantages of traditional holography as a 3D detection method and no pulsed laser, highly stable instruments or chemical post-processing is needed. The particle fields are detected in real time and accurately with facilities that can be miniaturized for ocean in situ detection[14,15]. This letter discusses the experiment of detection of underwater bubble fields with digital holography method.

Figure 1 shows the schematic diagram of the digital holography recording system of underwater bubble fields. This system is framed based on Mach-Zehnder interference., A semiconductor continuous laser is used whose wave length is λ=532 nm and maximum power is 100 mW. The laser beam is divided into two beams through a prism. The downward beam is made into a parallel light beam whose diameter is about 40 mm through the expander and collimator lens. This beam goes into the water tank vertically, enlightening the bubble field and being diffracted. The laser beam towards the right will be taken as the main reference beam after being expanded, collimated and reflected. As shown in Fig. 1, beams from 6 and 7 interfere at 8 with a little angle, and the interference fringe can be recorded by charge-coupled device (CCD). The holographic image of the field is then recorded by the CCD and saved in a computer. The CCD used in this experiment is the Apogee CCD U16m with a resolution of 4 096×4 096 (pixel) and the pixel size is 9×9 (μm).

The commonly used in-line digital holography was once applied in our early experiments. Mach-Zehnder inference holography is used later on and the results of them will be compared and discussed.

The transmission light field of a hologram exposed to inferred light $C(x, y)$ is

$$\begin{aligned} U(x,y) &= C(x,y)t(x,y) \\ &= t_{\mathrm{b}}C + \beta C|C|^2 + \beta R^* CO + \beta RCO^* \\ &= U_1 + U_2 + U_3 + U_4. \end{aligned} \tag{1}$$

There are four components of the above equation. If the

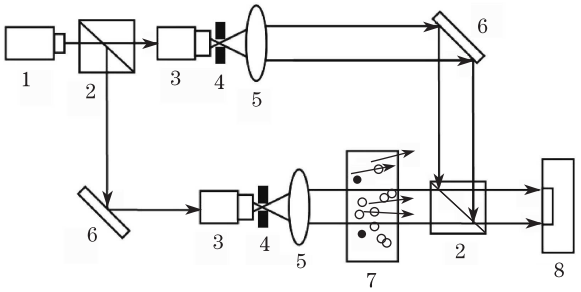

Fig. 1. Schematic diagram of digital holography optics based on Zehnder inference. 1: laser; 2: prism; 3: beam expander; 4: pinhole filter; 5: collimating lens; 6: mirror; 7: water tank; 8: CCD.

hologram is exposed to the original reference light wave, that is, $C(x,y)$=$R(x,y)$, the four components of the light field can be written as

$$\begin{cases} U_1 = Ct_{\rm b} \\ U_2 = \beta C|O|^2 \\ U_3 = \beta COR^* \\ U_4 = \beta CO^*R \end{cases}, \tag{2}$$

where $t_{\rm b} = t_0 + \beta(x,y)$, and β is a constant related to the photosensitive material which presents the relationship of exposure amount and transmittance. U_1 is the straight trans-illuminating part of the reference light. U_2 represents the self-coherent light of each light spot and the mutual coherent light of different light spots. $|R|^2$ is the intensity of the reference light and U_3 simply reproduces the original light except for a constant intensity given that the reference light is planar. When the original object light diverges, the conjugate light converges. Therefore, U_4 shows a real image that might be distorted due to the modulation of the reference light. If the hologram is illuminated with the conjugate of the reference light, that is, $C(x,y) = R^*(x,y)$, the third and fourth terms are U_3=$\beta R^*R^*O(x,y)$, U_4=$\beta|R|^2O(x,y)$, respectively. U_3 and U_4 are directly proportional to the object wave or the conjugate wave and thus a virtual or a real image is generated respectively. And the holographic reproducing of image is to determine U_4 using

$$u_z(x',y') = \frac{\exp {\rm j}kz_r}{{\rm j}\lambda z_r} \iint I(x,y)r(x,y) \frac{\exp {\rm j}k\sqrt{z_r^2+(x'-x)^2+(y'-y)^2}}{\sqrt{z_r^2+(x'-x)^2+(y'-y)^2}} {\rm d}x{\rm d}y. \tag{3}$$

In this experiment, in order to reproducing the image using Eq. (3) convolution method is involved, and Eq. (3) can be rewrite as

$$u_z(x',y') = [I(x',y')r(x',y')] * h_z(x',y'), \tag{4}$$

where

$$h_z(x,y) = \frac{\exp {\rm j}k\sqrt{z_0^2+x^2+y^2}}{{\rm j}\lambda\sqrt{z_0^2+x^2+y^2}}. \tag{5}$$

According to the Fourier transform, Eq. (4) can be writes as

$$u_z(x',y') = F^{-1}\{F[I(x,y)r(x,y)] \cdot H_z(u,v)\}. \tag{6}$$

For digital calculation, rewrite Eq. (6) in discrete form:

$$u_z(m',n') = F^{-1}\{F[(m,n)r(m,n)] * H_z(m'',n'')\}, \tag{7}$$

where $x = m\Delta x$, $y = n\Delta y$; Δx and Δy are the sampling interval along x and y axis. And in this letter, $\Delta x = \Delta y = 9$ μm, just the pix size of the CCD.

In Fig. 2, both the reproduced images of in-line holography and Mach-Zehnder holography are presented. In both images, the bubbles in focus have clearer and sharper edges than the others. By comparison between the two images, results can be found that: (1) by in-line holography method, the smaller bubbles have simple ideal clear edges, however the bigger ones have blur edges which will be difficult for auto detection and recognition; (2) by Mach-Zehnder method, both the smaller and bigger bubbles have clear edges that are ideal for auto-recognition. The Mach-Zehnder holography method is finally chosen in our experiment and the images are denoised through a self-adaptive filter.

The edges of bubbles in focus are sharp while those not in focus are blurred or even invisible, as shown in Fig. 3.

According to the bubbles edges, several edge-detection methods can be used for auto detection and recognition, such as Roverts, Sobel, Prewitt, and Canny. These methods are largely based on linear discrete convolution operations, but with different kernels designed to detect edges. Results with the four common edge detection methods are presented as Fig. 4, in which it can be found that both bubbles and other particles are detected and the bubbles edge is not always perfectly detected too. Thus these edge detection methods are not eventually adopted in our experiment.

The Hough transform is a feature extraction technique in the field of computer vision and image processing. The original Hough transform is used to detect lines in images, and later the Hough method has been extended to identify arbitrary shapes including circles. A circle can be presented by

$$(a-x)^2 + (b-y)^2 = r^2, \tag{8}$$

where (a,b) is the circle center, r is the radius of the circle, and (x,y) is any point in the circle edge. To identify

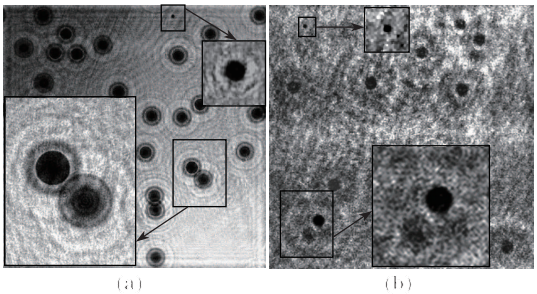

Fig. 2. Comparison of the tomographic images. (a) Reproduced by in-line holography; (b) Mach-Zehnder holography.

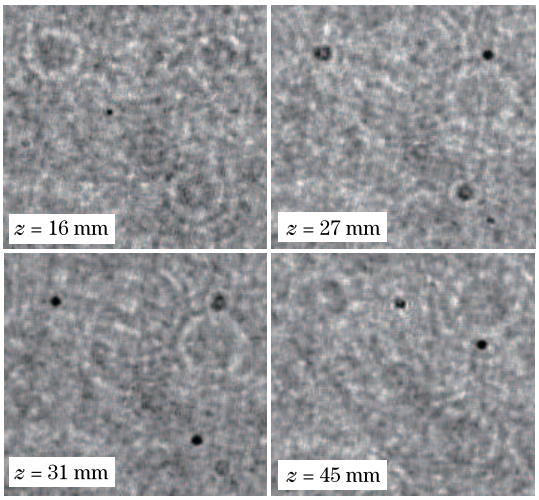

Fig. 3. Comparison of tomographic images produced with same x and y coordinates (same area) and in different z coordinates (different depths).

the circles in images, firstly an accumulator space is made up of a cell for each pix, initially each one will be set to 0. The parameter space is made up by

$$a = x - r \cdot \cos(t),\ b = y - r \cdot \sin(t),\ t \in [0, 2\pi). \quad (9)$$

Our goal is to count the vote of all points (x, y) and t values given a specific radius r. Calculate the voting and translate it into a 2D array (a, b) in the parameter space. The cell receiving more votes is more likely to be the circle center.

We use Hough transform instead of the common edge-detect method to pick up bubbles because Hough transform is appropriate to recognize and extract standard objects with simple shapes such as circles and therefore is suitable to deal with bubbles. The diameters of bubbles are set as parameters in the experiment to recognize and count the bubbles with different sizes. Figure 5 shows the recognition results of Hough transform. The bubbles are successfully recognized and extracted despite of the existence of other particles as well as noises.

After the whole tomographic image sequence is processed with Hough transform method, all bubbles are

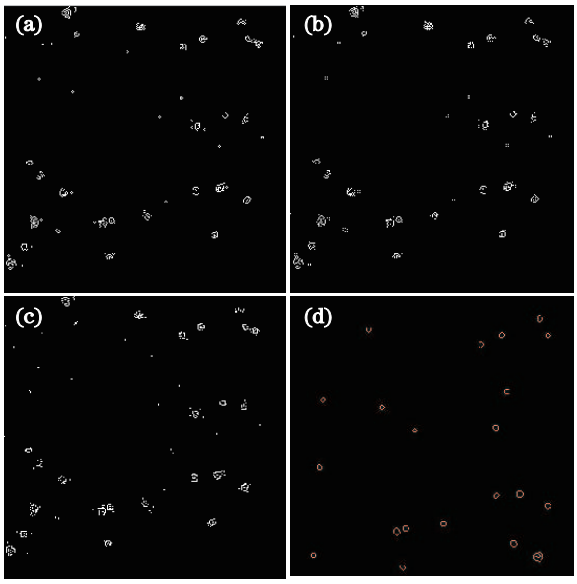

Fig. 4. Result of bubbles edge detection with commonly used arithmetic operators. (a) Sobel; (b) Prewitt; (c) Roberts; (d) Canny.

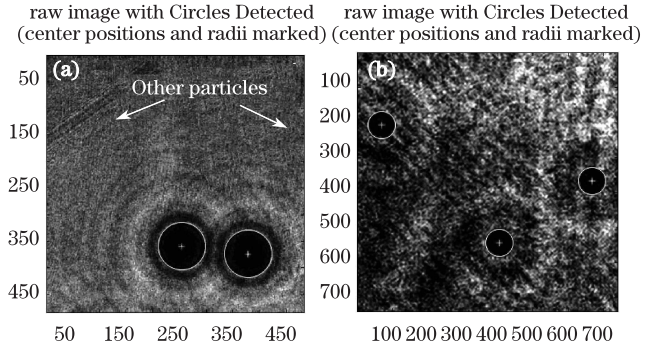

Fig. 5. Result of bubble edge detection and extraction with Hough transform. (a) With other particles existing; (b) with large amounts of noise.

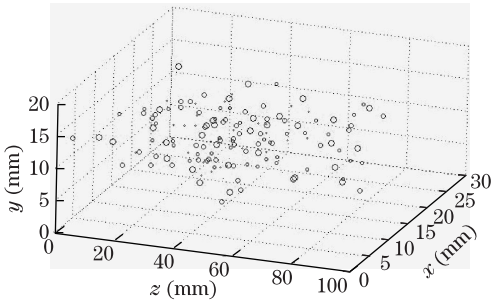

Fig. 6. 3D distribution of bubble space and size.

detected automatically while the size and position of each bubble are acquired and stored in a '.dat' file. With the data provided in the '.dat' file using 3D data visualization technique, a 3D distribution graph of bubble space and size is generated, shown in Fig. 6.

In conclusion, we study the space distribution of underwater bubble fields through the experiment that uses continuous laser and is based on Mach-Zehnder digital holographic system. The information on bubble sizes and space distributions are obtained by processing the hologram of the field. Our experiments show that digital holography is applicable for efficient, real time detection of under water bubble fields. This provides us with a new detection method and in-situ system for measurement of marine bubble fields.

References

1. B. D. Johnson and R. C. Cooke, J. Geophys. Res. C: Oceans **84,** 3761 (1979).
2. H. Medwin and N. D. Breitz, J. Geophys. Res. C: Oceans **94,** 12751 (1989).
3. J. Piskozub, D. Stramski, E. Terrill, and W. K. Melville, Opt. Express **17,** 11747 (2009).
4. D. C. Blanchard and A. H. Woodcock, Tellus **9,** 145 (1957).
5. P. A. Kolovayev, Oceanology **15,** 659 (1976).
6. S. A. Thorpe, T. R. Osborn, J. F. E. Jackson, A. J. Hall, and R. G. Lueck, J. Phys. Oceanogr. **33,** 122 (2003).
7. R. X. Cao, "Measurement and Analysis of Bubbles in Ocean surface layer and sub-surface layer", (in Chinese) PhD. Thesis (Chinese Academy of Sciences, 2006).
8. T. J. O'Hern, L. d'Agostino, and A. J. Acosta, J. Fluids Eng. **110,** 200 (1988).
9. W. Xu, M. H. Jericho, H. J. Kreuzer, and I. A. Meinertzhagen, Opt. Lett. **28, 164** (2003).
10. J. P. Fugal, R. A. Shaw, E. W. Saw, and A. V. Sergeyev, Appl. Opt. **43,** 5987 (2004).
11. L. Tian, N. Loomis, J. A. Domínguez-Caballero, and G. Barbastathis, Appl. Opt. **49,** 1549 (2010).
12. Q. Lü, C. Zhao, Z. Ma, B. Ge, Y. Gao, and Y. Zhang, Chinese J. Lasers (in Chinese) **37,** 779 (2010).
13. Q. Lü, B. Ge, Y. Chen, and Y. Zhang, Acta Optica Sinica (in Chinese) **31,** 0412009 (2011).
14. J. Watson, M. A. Player, H. Y. Sun, D. C. Hendry, H. P. Dong, in *Proceedings of Ocean'04. MTS/IEEE Techno-Ocean'04* **3,** 1248 (2004).
15. H. Sun, P. W. Benzie, N. Burns, D. C. Hendry, M. A. Player, and J. Watson, Phil. Trans. R. Soc. A **366,** 1789 (2008).